COMPUTER VISION AND IMAGE UNDERSTANDING
Vol. 66, No. 2, May, pp. 147–161, 1997
ARTICLE NO. IV970610

3D Voronoi Skeletons and Their Usage for the Characterization and Recognition of 3D Organ Shape

M. Näf and G. Székely

Communication Technology Laboratory, Swiss Federal Institute of Technology ETH, Gloriastr. 35, CH-8092 Zurich, Switzerland

R. Kikinis

Department of Radiology, MRI Division, Brigham & Women's Hospital, Harvard Medical School, 75 Francis Street, Boston, Massachusetts 02115

M. E. Shenton

Department of Psychiatry 116A, Harvard Medical School and Brockton VACM, 090 Belmont Street, Brockton, Massachusetts 02401

and

O. Kübler

Communication Technology Laboratory, Swiss Federal Institute of Technology ETH, Gloriastr. 35, CH-8092 Zurich, Switzerland

Received September 1, 1996; accepted January 9, 1997

The paper describes a procedure for the generation of the Blum skeleton (medial axis) of large, complex, digitized 3D objects. The proposed algorithm is a 3D generalization of the Voronoi skeleton concept, which is already in routine use for 2D shapes. A specific algorithm for the generation of 3D Voronoi diagrams of very large point sets (containing several 100,000 generating points) is described. The pitfalls and drawbacks of pruning procedures are discussed, and a topologically correct regularization algorithm is given for the necessary regularization of the resulting Voronoi diagram. The performance of the developed procedures is illustrated on synthetic objects as well as on large, complex anatomical data, e.g., the segmented white matter of a human brain extracted from MR data. © 1997 Academic Press

1. INTRODUCTION

Analysis of organs in 3D radiological data calls for shape description methods which are capable of dealing with the variability and complexity of the human anatomy including organs of extremely complex shapes like the human brain. Our investigations will concentrate on the following two different aspects of organ shape analysis:

• Recognition of organs of the human anatomy in 3D radiological data. We will concentrate especially on the aspect of finding robust methods for matching generic anatomical knowledge coded in anatomical atlases with individual anatomy found in acquired radiological data. The basic problem of such interindividual anatomical matching is that while brains are very similar in their overall shapes, the surface of individual brains (i.e., the structure of sulci and gyri) is fingerprint-like; no two brains are the same. This makes classical, surface-based methods fairly useless and we must search for methods which are able to separate the general global brain shape from the individual variations in a well-controlled and robust way.

• Analysis and characterization of the morphological structure of the cortex. This problem is complementary to the first one in the sense that here we do not care about generic shape characteristics but want to analyze the unique individual variations.

One has to realize that the requirements for the shape descriptor to be used are actually complementary for these two cases.

• In the first case we regard the different objects as samples of a population. An ideal object shape descriptor would allow us to search for the common properties of the object class without being much disturbed by the individual variations of the single entities. In other words we are looking for methods capable of describing *global*, general shape.

• In the second case we will investigate how the individual differs from other members of its class. We will characterize its unique, distinctive features. For this purpose we

1077-3142/97 $25.00

need a shape descriptor which can code and handle *local*, specific details efficiently.

The concept of local symmetry, originating from the pioneering work of Blum [2] has the potential of unifying these requirements for the description of biological objects. The shape descriptor resulting from a skeletonization process consists of hierarchically organized local symmetry axes, allowing task-dependent differentiation between global object shape and local individual features. We will also investigate how serious limitations of the skeletal representation can be potentially eliminated by generalizing the concepts of Blum to a collection of all local symmetries of a scene and how skeletons and the multi-scale medial axis concept of Morse *et al.* [12] can be possibly combined to a powerful tool for object recognition in complex anatomical scenes.

2. VORONOI SKELETONS IN 2D

During the past two decades skeletonization has been an important research area for image processing and computer vision, concentrating primarily on the basic problem of how the MAT concept could be implemented on the digital image raster. As rotational invariance is essential for reliable shape description, an Euclidean metric (or a reasonable approximation of it) must be reconciled with the raster-type connectivity during the skeleton generation procedure.

An elegant way to generate topologically, as well as geometrically, correct skeletons is the reformulation of Blum's concept in a semicontinuous way. Objects on the raster plane can be faithfully represented by their discrete boundary points, providing the densest possible sampling of their (unknown) continuous outline [4, 14, 16, 19]. The Voronoi diagram of these boundary points is a superset of the MAT [4] and can be generated very efficiently [14]. The Voronoi Diagram (VD) is a fundamental structure in computational geometry. It is defined on a set S of n points in d-dimensional Euclidean space E^d. The points of S are called sites (sometimes other basic elements, e.g., polygons, are used as sites). The VD of S splits E^d into regions with one region for each site, so that the points in the region for site $s \in S$ are closer to s than to any other site in S. The Delaunay triangulation (DT) of S is the dual of the VD. It decomposes the convex hull of S into a number of convex cells having elements of S as vertices. Each cell has the property that its vertices lie on a d-dimensional circumscribing ball and that there are no other sites lying inside this ball. More details on VD and DT can be found in [15].

Several regularization procedures have been proposed to reduce the resulting 2D VD to its stable, essential parts (pruning). They can most easily be understood by referring to the straight line dual of the VD, the DT. The object can be envisaged as being composed of Delaunay triangles. The goal of regularization is to identify those peripheral Delaunay triangles which are irrelevant for representing the object at coarser scales, and to suppress the corresponding parts of the VD in order to obtain the desired Voronoi skeleton. Note that each Voronoi edge corresponds to a Delaunay edge and that each Delaunay edge cuts the object into two parts. Hence the subpart that by this Delaunay edge is cut away from the object can be used to measure the importance of the corresponding Voronoi edge. Removing this subpart from the object means also replacing a piece of the object's original outline by the cutting Delaunay edge (cf. Fig. 5).

Several procedures have been proposed to measure the relevance of the different branches of the VD:

- Brandt and Algazi [4] use the maximal distance between the original outline segment of the object and the Delaunay-edge it is replaced by;
- Ogniewicz and Ilg [14] calculate the difference in length between the original outline segment and the Delaunay edge; and
- Meyer [11], Talbot and Vincent [19], and Attali and Montanvert [1] propose using the angle between the fire-fronts which meet at the selected skeleton branch. It can be easily shown that the ''pointedness'' of the appropriate Delaunay triangles provides the same measure.

While it has been shown that the inner VD of the boundary points is topologically equivalent to the skeleton of the object [16], simply thresholding the branches will not necessarily preserve the topology of the VD, that is the topology of the original object. In order to be sure that no topological changes happen, another regularization approach must be taken. The deletion of Delaunay triangles can be made in a recursive manner by deleting only those triangles on the border (i.e., those having two sides on the actual outline of the object, and one side through the object) which ensures that the graph topology remains unaltered.

Recursive regularization algorithms also need a measure which decides where the consecutive deletion of triangles has to stop. All kinds of measures (such as the previously discussed ones) can be used for this purpose. The recursive deletion ensures that no topological changes occur. Note, however, that the first two of the proposed measures change monotonically during the successive deletion procedure; therefore, simple thresholding will also guarantee the preservation of the topology. This is not the case for the third (pointedness) measure, which means that it must be combined with a recursive deletion algorithm. In this case, however, small pointed triangles on the object boundary can block the regularization process, in effect making irrelevant branches of the VD undeletable. This is a general problem of nonmonotonic regularization measures.

In the following we will study the 3D generalization of the skeleton. In contrast to the 2D case, only few studies have been published [1, 3, 13, 18]; consequently, many theoretical and implementational problems remain unsolved. While the generation of the 3D VD of very large point sets poses ''only'' technical difficulties, no satisfactory procedure for 3D pruning has been proposed. We discuss the 3D generalization of some 2D regularization measures and show preliminary results.

3. 3D VORONOI SKELETONS

3.1. *Skeletons in 3D*

The analysis of real 3D image scenes requires methods capable of dealing with the shape of truly 3D objects. Such scenes arise, e.g., in medical image analysis, where current radiological image acquisition techniques deliver high-resolution true 3D images of the individual patient anatomy. Traditional slice-by-slice methods are generally misleading and especially troublesome if dealing with object shape. Computer representation and handling of biological objects calls for 3D shape analysis methods dealing with the complexity and variability of the anatomy. Such techniques may find broad application in image analysis (e.g., for computer representation and manipulation of anatomical knowledge) as well as in computer graphics (e.g., for efficient manipulation and deformation of 3D objects). Skeletonization (originally emerging from the analysis of the morphology of biological objects) appears to be one of the few promising techniques to achieve these goals.

The MAT concept of Blum can be generalized straightforwardly to 3D. Usually, the fire-fronts initiated at the boundary of an object meet on surfaces, resulting in a skeleton consisting of branched 2D manifolds. However, in degenerate cases (as, e.g., perfectly cylindrical objects) the quenching procedure will produce curves instead of surfaces. As we do not want to make any a priori restrictions on the shape of the object investigated, the skeletonization algorithm should be able to generate 3D skeletons that contain both surface (2D) and lineal (1D) parts.

The basic theoretical results behind the 2D Voronoi skeleton generation procedures [4, 16] can also be generalized to 3D. The strategy to be followed is then analogous to 2D: the boundary of the object to be analyzed is sampled, the VD of the sample points is generated, and finally the irrelevant branches must be pruned to get the 3D Voronoi skeleton which is a reasonably good approximation of the continuous skeleton. It must be noted that the proven theorems require a maximally dense sampling, i.e., sampling the boundary at voxel level. Due to the enormous algorithmic difficulties caused by the huge amount of boundary points in a maximally dense sampling, some proposals have been made for sparse boundary sampling. It seems to be intuitive to generate less dense sampling on surface patches with low local curvature. Such approximations, however, are only admissible if the object is approximated by polygons, in which case entirely different algorithms for the generation of the skeleton of continuous objects must be found [10]. Otherwise, in addition to large distortions in the skeleton algorithmically disturbing side-effects have to be expected as, e.g., parts of the inner skeleton may become disconnected.

3.2. *3D Voronoi Diagram Generation*

Maximal sampling of the boundary of 3D objects on a 256^3 image raster usually results in several 100,000 generating points. Unfortunately, the extremely efficient 2D VD generation algorithm has no direct generalization to 3D because it takes advantage of the explicit ordering of the edges incident in a vertex which is given in 2D but not in 3D.

In computational geometry many algorithms for 3D VD generation have been proposed and some implementations are available. Most of them, however, run into serious problems when faced with such a large number of generating points. In addition, they are usually unable to handle degenerate cases caused by more than four cospherical points; a situation that is unavoidable among point samples located on a regular image raster. Handling cospherical points calls for more flexible data structures to represent a DT consisting not only of tetrahedra but of general convex polyhedra.

In our implementation we extended an existing algorithm [5] adapting it to deal with cospherical input points and supplying it with a uniform grid for fast point location, a technique which is well known from computer graphics applications. The algorithm actually computes the DT of a point set which is the dual representation of the VD. It is based on the divide and conquer (D&C) paradigm, which basically consists of recursively applying two phases: a subdivision of the problem into subproblems and a merging of the subproblems' solutions. The efficiency of the D&C algorithm depends on an efficient merging of the local DTs computed in the previous phase. The merging requires a number of local modifications on both DTs which is an expensive task. This can be avoided if instead of merging partial results in a second step, the merging part of the DT is built first, and then the independent parts of the DT are computed on subsets of the input points.

We have chosen to follow Cignoni's algorithm both for its time characteristics (it can be parallelized and has been proved to be optimal in 2D both in terms of mean and worst time complexity) and its memory requirements: the Delaunay polyhedra can be stored to disk immediately when they are generated and only a relatively small list of Delaunay faces have to be retained in memory.

The local DTs are generated by successively constructing

new Delaunay polyhedra from already computed Delaunay faces. For that a new vertex must be searched in the input point-set so that together with the Delaunay face it forms a new Delaunay polyhedron. This operation can be speeded up considerably if one uses the fact that in most cases one has to search the missing vertex only among a limited number of points when choosing an appropriate scanning of the space. In fact the missing vertex must lie on the other side of the Delaunay face and within a sphere of unknown radius which passes through the corner vertices of the Delaunay face. Hence a sequence of such spheres with increasing radius can be generated and the space inside of them scanned until the missing vertex is found. The uniform grid, in our case a regular, nonhierarchical partitioning of the 3D space in cubic grid cells, is used as an indexing scheme for fast selection of points contained in a given sphere. To avoid sphere to cell conversion the search is performed in the smallest circumscribed cube of the sphere.

The VD can be directly obtained from the DT by the following substitutions. Each Delaunay polyhedron becomes a Voronoi vertex located at the center of the polyhedron's circumsphere. Each Delaunay face becomes a Voronoi edge joining the circumsphere centers of the two Delaunay polyhedra which are in touch over that face. Finally each Delaunay edge becomes a Voronoi face made up of all the Voronoi vertices representing the Delaunay polyhedra which meet at that edge.

With our implementation we have been able to generate 3D VD's of large medical objects with over 250,000 boundary points.

3.3. *Regularization*

As discussed in the 2D case, the regularization needs:

- a measure expressing the significance of a Voronoi branch;
- a deletion sequence ensuring topology preservation.

The inner VD of the generating boundary points has a special structure in 2D. For a simply connected object without holes it is an acyclic graph representing a tree. Hence every Voronoi edge connects exactly two parts of the graph. This enforces a hierarchy between branches, defining a natural deletion sequence when progressing from the outmost branches to the inside of the graph. Equivalently every Delaunay edge (the dual counterpart of a Voronoi edge in 2D) cuts the object into two disjoint parts. This allows easy definition of significance measures based on 2D form considerations, expressing the importance of the removed subpart for the overall appearance of the object. These nice properties lead to the definition of different significance measures in 2D, making simple regularization techniques as discussed in the previous section applicable. Note that the situation for an object with holes is similar since the cycles that will show up in the Voronoi graph reflect the object's topology and therefore must be preserved anyway.

In 3D, however, the Voronoi graph rather resembles a net containing many cycles and thus lacks the hierarchical organization which has been proved so useful in 2D. This means that there is no natural deletion sequence, uniquely defined by the topology of the cell complex. It can be shown that apart from trivial degenerate cases, there are always many substantially different deletion sequences of the Voronoi faces equally respecting the topology of the object. As no theoretical results are known about the effect of the deletion sequence to the resulting skeleton, the uniqueness of the resulting skeleton may be questioned. There is of course no difficulty in defining arbitrarily a partial ordering, e.g., on Voronoi faces but in general it is hard to find an ordering which ensures the invariance of the skeleton after pruning.

During the recursive regularization procedure the DT or equivalently the VD is stepwise reduced by deleting single Delaunay polyhedra when operating on the DT or Voronoi faces when operating on the VD. In both cases the dual representation is updated; i.e., the deletion of a polyhedron on the DT implies the deletion of its corresponding vertex on the VD. The sequence in which those elements are removed is called the deletion sequence. The deletion sequence must ensure that after each step the remaining part of the DT is topologically equivalent to the original object. For this purpose different checks for topological equivalence have to be implemented either on the DT or on the VD. In the following, the topological check for Delaunay polyhedra will be described.

The theory of cell complexes, as already used in image processing by Kovalevsky [9], provides a powerful tool for the investigation of the topological properties of finite sets. The Delaunay tetrahedralization can be modeled as a cell complex consisting of the Delaunay polyhedra and their bounding elements. As the deletion of a single Delaunay cell p_i changes the boundary of the actual cell complex $\mathscr{D}_i$ only locally, namely at the bounding elements of p_i, the topological equivalence of the cell complex before ($\mathscr{D}_i$) and after its deletion ($\mathscr{D}_{i+1}$) can be decided locally by the following deletability criterion.

Consider the bounding elements of p_i. They can be grouped into two categories according to whether they belong to the boundary of the current subcomplex $\mathscr{D}_i$ or whether they are cutting through it. The elements which belong to the boundary are called outside elements; the others are called inside elements. In Fig. 1 a polyhedron has been cut out from some cell complex as an example. The inside faces are shaded in light gray and the inside edges are the dashed lines. There are no inside vertices (in our case this is generally true since the vertices have

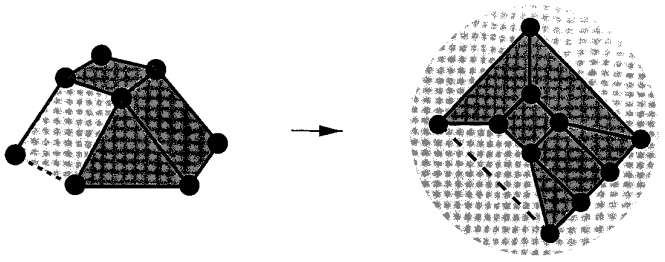

FIG. 1. Subdivision of the surface of a Delaunay polyhedron into outside (dark) and inside (light) elements. On the left the original polyhedron is shown; on the right the surface is mapped onto the plane (one of the faces has been cut open by mapping one of its points onto the circumcircle of the figure).

been chosen from the boundary of the initial cell complex). The outside faces are shaded in dark gray, the outside edges are the solid lines, and all the vertices are outside vertices. In order to have a complete picture of the situation a plane model of the polyhedron is given on the right-hand side (the boundary of the circle corresponds to a single point of an inside face). The cells can be grouped into connected components containing only inside or only outside elements. The deletability criterion is defined by two conditions:

1. There is exactly one inside and one outside component.
2. The boundary between the two components is a non-self-intersecting, closed line.

The criterion is illustrated with the two examples given in Figs. 1 and 2. In both examples there is exactly one inside and one outside component, but in the second example their common boundary is self-intersecting at point $\mathcal{Q}$. Consequently p_i is deletable only in the first example and not in the second one. The given criterion is clearly sufficient to guarantee topological equivalence, as the remaining outside and inside face elements of p_i make up exactly two topologically equivalent components, even after the removal of their common boundary.

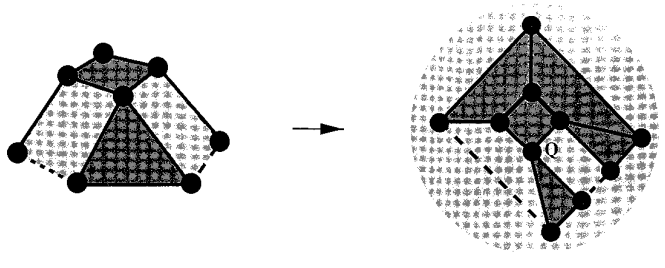

FIG. 2. The surface of a Delaunay polyhedron shown in 3D (left) and its surface mapped onto the plane (right). The polyhedron is nondeletable as the boundary line between the inside (light) and outside (dark) components is self-intersecting at point Q.

```
function is_deletable(p_i)

1.  oi_edgs = make_list()
    oo_edgs = make_list()
    boundary = make_list()
2.  FOR each outside face f_i ∈ p_i DO
      FOR each edge e_i ∈ f_i DO
3.      IF member(e_i,oi_edgs)
          remove(e_i,oi_edgs)
          insert(e_i,oo_edgs)
        ELSE
          insert(e_i,oi_edgs)
4.  FOR each inside face f_i ∈ p_i DO
      FOR each outside edge e_i ∈ f_i DO
5.      IF not member(e_i,oi_edgs) and
          not member(e_i,oo_edgs)
          RETURN not deletable
6.  IF size(oi_edgs) > 0
7.    e_0 = get_edg(oi_edgs)
      v_0 = start_vrt(e_0)
      v_i = end_vrt(e_0)
8.    insert(v_0,boundary)
9.    WHILE (e_i=get_edg(oi_edgs,v_i))>0 DO
10.     IF member(v_i,boundary)
          RETURN not deletable
11.     insert(v_i,boundary)
12.     IF start_vrt(e_i) == v_i
          v_i=end_vrt(e_i)
        ELSE
          v_i=start_vrt(e_i)
13. IF size(oi_edgs) > 0
      RETURN not deletable
14. o_vrts = make_list(boundary)
15. FOR all e_i ∈ oo_edgs DO
      insert(start_vrt(e_i),o_vrts)
      insert(end_vrt(e_i),o_vrts)
16. IF size(o_vrts) == nr_of_vrts(p_i)
      RETURN deletable
    ELSE
      RETURN not deletable
```

FIG. 3. Pseudo-code of the algorithm deciding the topological deletability of a Delaunay polyhedron.

In Fig. 3 the deletability criterion is given in pseudo-code. The function takes a polyhedron p_i as input and returns a boolean value depending on whether p_i is deletable or not. Let us step through the algorithm:

lines 1–3. Two lists of outside edges are filled. The list `oo_edgs` holds the edges bounding two outside faces, the list `oi_edgs` those bounding an inside and an outside face.

lines 4–5. Outside edges bounding two inside faces are then detected. If such edges are found the function can immediately return with a negative answer. Notably this addresses not only the case of one-dimensional but also two-dimensional components with a boundary that is self-intersecting along an edge.

lines 6–12. One of possibly several component boundaries

is constructed as follows. An arbitrary edge is taken from the list `oi_egs` (function `get_edg ( )`), one of its vertices (v_0) is added to the list `boundary` and the other (v_i) used to retrieve the next edge (e_i) starting at v_i with the function `get_edg ( )` . After a test whether the vertex v_i of the new edge is already part of the component's boundary, and therefore the boundary would be self-intersecting (line 10), v_i is added to the list `boundary` (line 11). This is done repeatedly until the component's boundary is complete.

line 13. At this point the list `oi_edgs` should be void, otherwise there are more than one outside components.

lines 14–16. The last check is whether all vertices make part of the single outside component we found. This is done by collecting all vertices belonging to outside edges in the inner of the component and the vertices of the component's boundary in the list `o_vrts`. If `o_vrts` contains all vertices, p_i is deletable otherwise it is not.

In 2D a deletion sequence has been defined by the special hierarchical structure of the DT. It was similar to a peeling of the object. One layer of deletable triangles after the other has been removed from the object. Triangles of the same layer were independent from each other and got the same order number. In 3D the topological structure of the cell complexes is more complicated. This leads to configurations where the deletion of a polyhedron from a layer of potentially deletable polyhedra makes another polyhedron of the same layer nondeletable. This fact shows that one will have to (more or less arbitrarily) choose one of several possible deletion sequences. We would like the deletion sequence to approximate best possible an isotropic peeling of the object like in 2D. This requirement has driven the design of the algorithm shown in Fig. 4, which produces two possible deletion sequences (paths (a) and (b)).

The function `is_deletable ( )` can be used to determine the current layer of deletable polyhedra. These are put into a processing queue. Then one polyhedron after the other is taken from the queue and tested whether it is still deletable. If it is, it is removed from the queue, otherwise reinserted at the end of the queue. All polyhedra which are removed from the queue receive the same sequence number. When no more polyhedra in the queue are deletable, the queue is cleared and a new layer of polyhedra established. Note that the order in which the polyhedra are put into the queue will eventually influence the outcoming deletion sequence since the deletability of a polyhedron can change while it is in the qeue. In practice the polyhedra are inserted randomly and this effect is neglected. Both generated deletion sequences are similar to

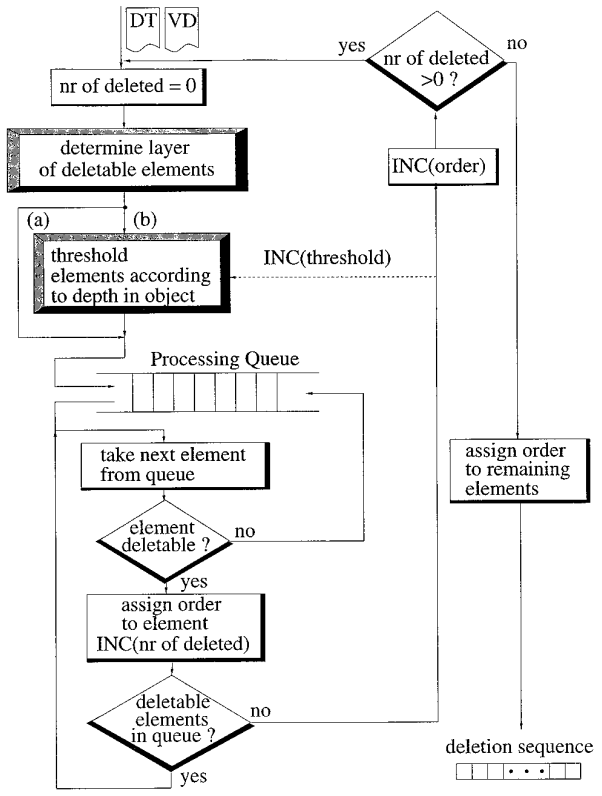

FIG. 4. Flowchart of the algorithm determining the deletion sequence of the Delaunay cells during the pruning procedure.

a peeling of the object. The first one (a) just depends on the DT's topology. To produce the second one (b) only elements up to a certain depth in the object are considered in each layer. The depth in the object of a polyhedron is measured by the radius of its circumsphere. This leads to a more isotropic peeling of the object.

During the regularization the polyhedra, ordered according to the deletion sequence, are removed from the object one at a time as long as two requirements are fulfilled:

- They are still deletable and not blocked by neighboring polyhedra at which the regularization has already been stopped.
- Their significance (determined by a significance measure as described below) is less than a chosen threshold.

The generalization of some significance measures from 2D to 3D is not straightforward. We will distinguish global and local significance measures. A local measure of an element is only influenced by those boundary points which either are taking directly part in the formation of this element or have such points in their neighborhood. A global measure of an element is defined on a subpart of

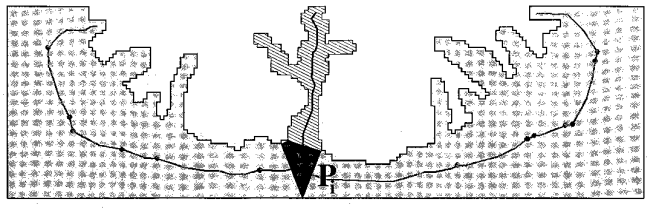

FIG. 5. Interpretation of the global significance measure in 2D through part–subpart decomposition of the object. The Delaunay triangle P_i is associated with the protrusion denoted by the dashed area. The importance of the Delaunay triangle (and the associated Voronoi vertex) can be expressed by measuring the significance of this subpart for the overall shape of the object.

the shape assigned to that element (see Fig. 5). In the figure the hatched part of the object is the subpart assigned to the polygon P_i. Here we use the fact that in 2D the edge of the polygon dual to the Voronoi edge to be characterized cuts the object in two. In 3D a Delaunay face generally does not cut the object into two parts, making the definition of measures based on part-subpart comparisons more complicated than in 2D. A possible solution is to use a cutting surface composed of faces from *several* Delaunay polyhedra that have already been removed instead. Such a cutting surface cannot, however, be defined uniquely based solely on the topology of the cell complex, as already discussed above. In addition, the resulting cutting surface can become fairly complex and the question arises whether the substitution of the original outline with that cutting surface is really a simplification of the object.

Local measures as the ''pointedness measure'' based on the angularity criterion can be easily generalized to 3D by measuring 3D angles of the Delaunay tetrahedra [1]. For general convex polyhedra, however, it is not evident how to generalize the angular criterion. Therefore, we propose an alternative measure based on distance ridges, which is related to the angular criterion.

According to the definition of the MAT by the centers of all maximal inscribing spheres, the skeleton of an object is equivalent to the ridges of its distance map (DM). Euclidean DMs can be generated very efficiently following, e.g., a sequential algorithm proposed by Danielsson in 1980 [6]. In the past it has already been tried to extract ridges directly from DMs, but the connectivity of the resulting skeleton is not guaranteed. Hence several approaches tried to join the separated portions of the skeleton in a postprocessing step, which turns out to be a very difficult task already in 2D.

The strength of the ridges in the DM, however, can well be used for the characterization of the significance of single Voronoi faces. While the usage of such measures has been proved to be very difficult for the extraction of ridges from distance maps from scratch, the characterization of skeletal sheet candidates based on the ridge strength is a much easier problem, as the Voronoi faces not only specify the exact position of the ridge to be investigated, but even define the orthogonal direction to it.

The ridge-strength measures is a combination of the information at hand from the VD (i.e., exact location and orientation of possible skeletal faces) and the information derived from the DM (how well a candidate face represents a ridge in the DM). The quality of a ridge can be described at every point of a candidate face by the local curvature found in the DM in direction of the face's normal. One has to note here that in general ridges will not always be faces; the skeleton will converge to lines where the object's shape shows radial symmetry. An analysis of the Hessian matrix of the DM can be used to determine the type of the local object symmetry. The number of its eigenvalues that are almost zero corresponds to the dimensionality of the ridge. This way the dimensionality of the skeleton can be determined locally without any prior decision about the expected object shape.

We used the above procedure to generate skeletons of different artificial test objects. Some results, cuboids, cylinders, and their composition are shown in Fig. 6.

4. SKELETON BASED OBJECT RECOGNITION

Skeletal description of 3D objects offers a solution to cope with problems of description and analysis of complex shapes. Practical application of this methodology for object recognition is, however, impeded by the following fundamental problems:

• The calculation of the hierarchical skeleton will be, even after solving the open problems discussed in this paper, computationally expensive and algorithmically complex. This means that the use of skeletal shape description in 3D must be restricted to cases where approximation techniques are feasible, or where the additional information provided by the skeletal description (basically the hierarchical organization of the shape) is really necessary, justifying the large additional costs against simpler (e.g., surface based) methods.

• The methods discussed for skeletonization require a binary object for the analysis, which necessitates prior segmentation of the scene. In some cases, however, segmentation can be difficult, making the routine application of skeletal analysis illusory.

• The idea of skeletonization only produces a (small) part of the full set of local symmetries of an object. Large parts of the general symmetry information about the object are suppressed by the procedure. This can be easily seen in the case of a rectangle, where the formation of the symmetry axes of the two smaller sides is blocked by the ''quicker'' burning up between the longer sides. This feature is essential for the skeletal description and is mainly

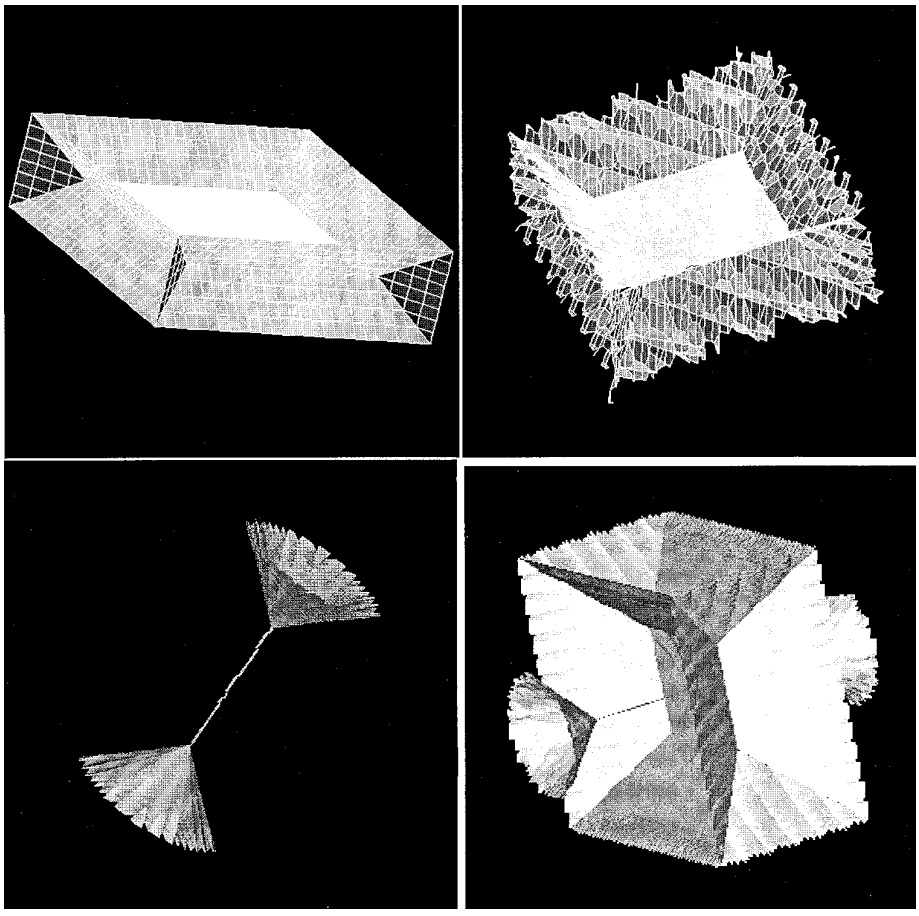

FIG. 6. 3D Voronoi skeletons of artificial objects. Top left, skeleton of a cuboid. Top right, the same cuboid rotated by $\phi = 15°$, $\theta = 65°$, illustrating the invariance of the resulting skeleton on oblique rotation. Bottom left, elongated cylinder (due to rotational symmetry, the object is represented by a midline instead of a medial surface with the exception of the cones generated by the closing faces). Bottom right, the union of a cuboid and a cylinder.

responsible for the branching topography which is the basis of the skeleton hierarchy. On the other hand, changes in the object which deeply influence the burning pattern will result in basic reorganization of the skeletal branches. The notorious sensitivity of skeletons to topological noise is a well known consequence of this, and we expect this situation to be even worse in three dimensions. The mutual position of objects (e.g. objects embedded one in another or touching one another) in a complex scene will lead to similar changes in the object's skeleton. This problem can only be avoided if the objects are segmented and isolated before skeletonization. This requirement may make skeletons nearly useless for the recognition of objects in complex scenes.

Calculation of symmetry transforms of images using mixed wave/diffusion processes [17] or the multi-scale medial axis (MMA) transformation [12] offers an appealing way to cope with many of the above-mentioned problems. The basic idea of this general symmetry transformation is the propagation of edge information into the object, creating local symmetry or medialness information where evidence generated by opposite object boundaries accumulates without terminating front propagation at quenching points. These methods can process directly gray-valued images and also allow the boundary points to participate in any number of symmetry relations. This way one gets the complete symmetry set without the suppression effect observed in the MAT transformation.

Figure 7 shows the 3D medialness field of a binary rectangle, as generated by the MMA transformation. The single images illustrate the medialness information on different scales. The images demonstrate that both symmetry axes between the long and the short sides survive, providing complete information about the symmetry of the original object.

The different symmetry axes can be found as 1D ridges in the 3D medialness space (note that the medialness field has an extra dimension in addition to the spatial one, the scale). Figure 8 shows the result of ridge extraction in the

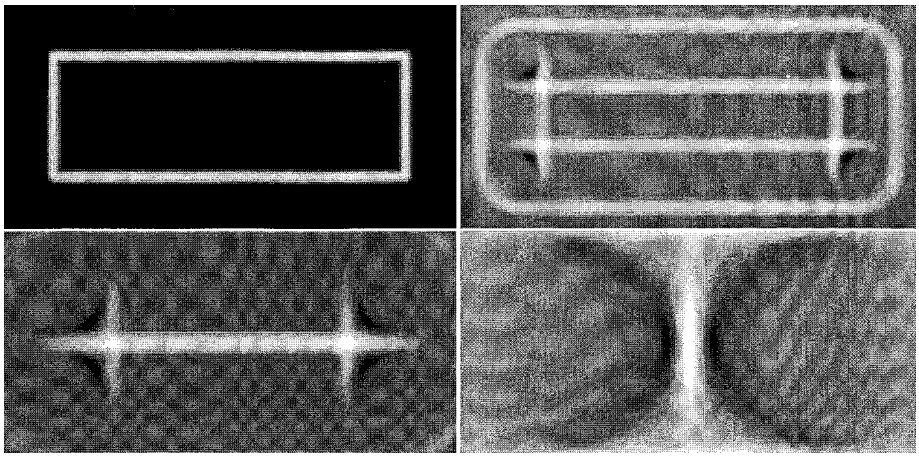

FIG. 7. Generation of the medialness scale-space of a rectangle. The top right image shows the edges of the original object, used to initialize the wave/diffusion process. The figures from left to right and top down show the result of the wave propagation at growing times. The bottom right image captures the time of the formation of the symmetry axis between the long sides, while the symmetry axis between the short sides is shown on the bottom right figure.

3D medialness field and a projection to the plane of the spatial coordinates. One can clearly see the classical skeleton as part of the symmetry structure, while the remaining symmetries have also been constructed.

The mixed application of the MAT and this general symmetry transformation opens a promising way for using skeletons in object recognition and matching. In many applications (as, e.g., anatomical atlas matching) it is reasonable to create a model of the objects under investigation. As the model is created only once, the amount of work required for its generation is not critical. The MAT of such a model can be produced by the methods discussed in the previous section, creating a structured description of the object. For an object to be recognized in a complex scene the MMA transformation of the whole scene can be generated, and we can try to fit our skeletal model elastically onto the resulting ridges the same way, as we identify the skeleton of the rectangle in the medialness field. Generalizations of the well-known snakes [7] offer a possible way to perform this kind of matching.

5. SKELETAL CHARACTERIZATION OF ORGANS BASED ON 3D RADIOLOGICAL DATA

We illustrate the power of skeletal representation on two prototypical medical applications. In the first case bone thickness in the acetabulum has to be investigated for optimal prosthesis placement in hip joint replacement operations. In the second example the generation of skeletons of a human brain extracted from 3D MRI data will be demonstrated.

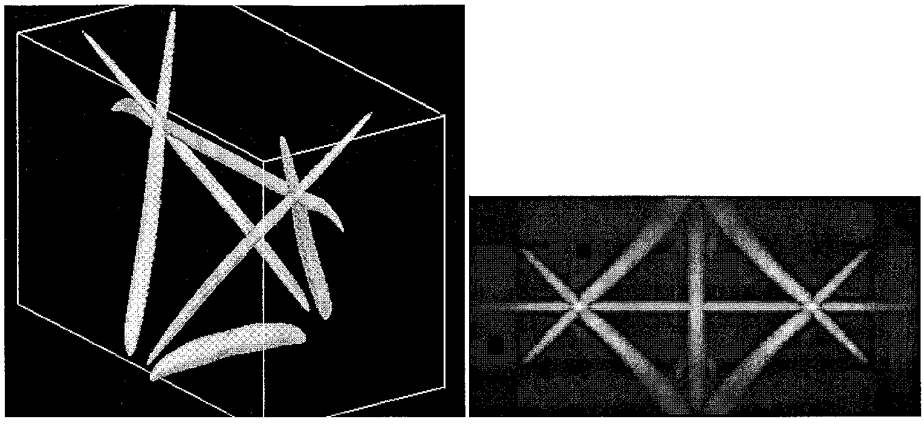

FIG. 8. Ridges in the 3D medialness field of a rectangle. The left figure shows the resulting ridges as an isosurface in the medialness space, while on the right image the detected ridge strength have been projected to the subspace of the spatial coordinates using maximum intensity projection.

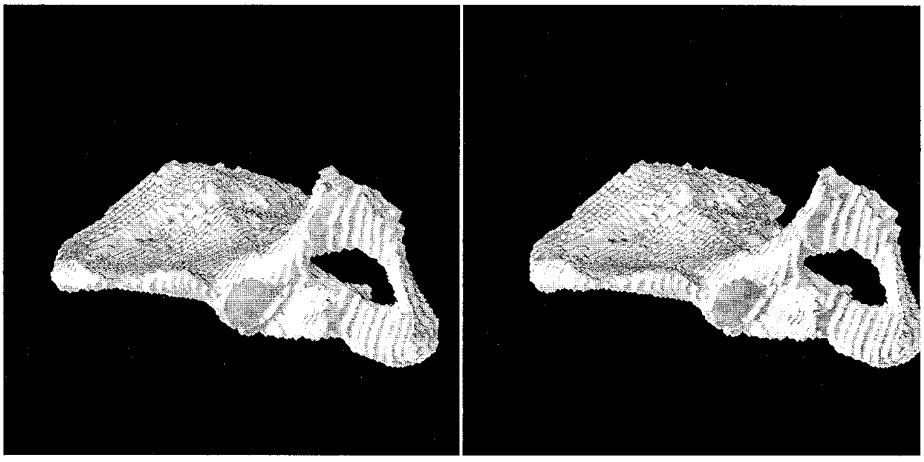

FIG. 9. Fusible stereo pair of the 3D rendered hip bone under study.

5.1. *Bone Thickness Characterization Using Skeletonization*

Optimal placement of hip joint replacement prosthesis requires general knowledge about the thickness of the surrounding bone structures. Such knowledge can be extracted from the analysis of the anatomical variation in a selected training population. Quantitative evaluation, however, is not possible without adequate representation of the hip bone. Skeletal description provides a natural basis for this analysis and proved to be useful for the characterization and visualization of the thickness of the hip bone around the acetabulum.

Figure 9 shows a 3D rendering of a hip bone to be analyzed. The dataset contained 49,733 boundary points, which produced 65,073 Delaunay polyhedra and 102,447 elementary Voronoi faces. After a first regularization step using the ridge strength as significance measure 29,928 elementary Voronoi faces were left. The remaining faces

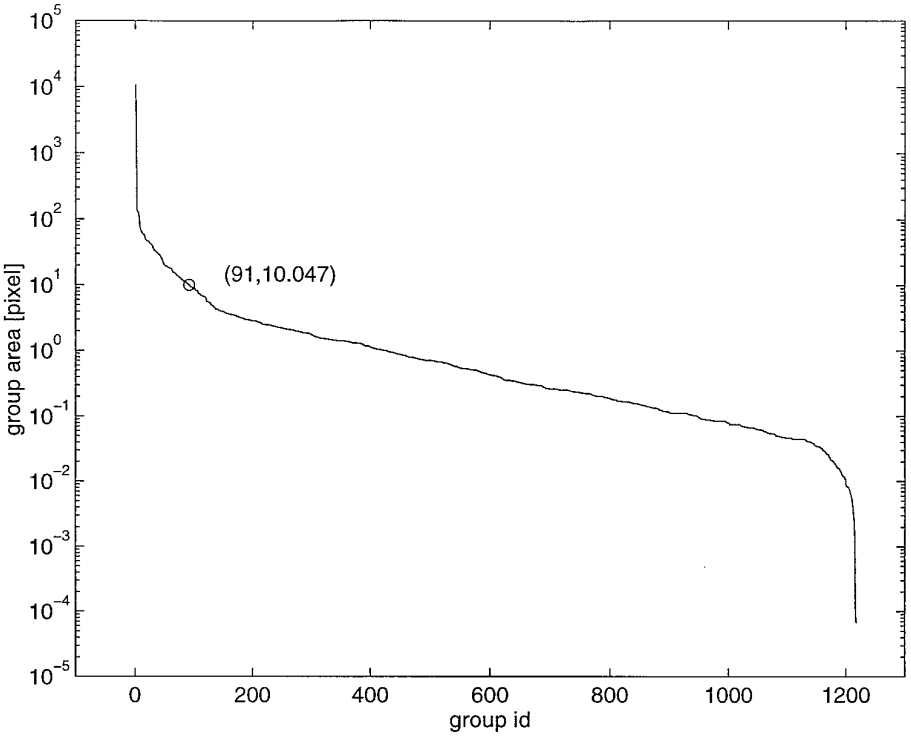

FIG. 10. Distribution of the overall area of the face groups making up the hip bone skeleton resulting from the first regularization step.

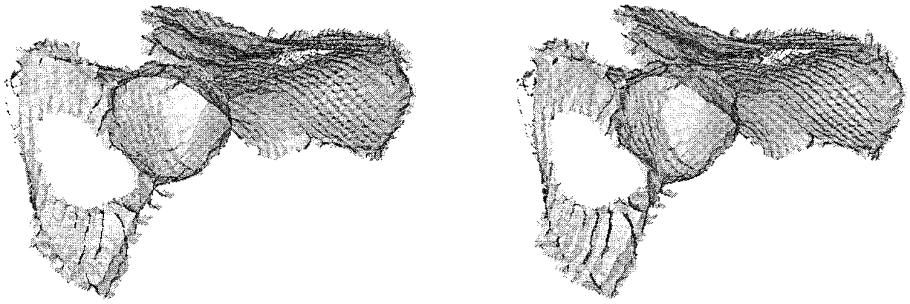

FIG. 11. Fusible stereo pair of the 3D rendered skeleton generated automatically from the hip bone under study using regularization and Voronoi face grouping.

can be sewn together at edges where only two of them meet. This aggregation of individual faces into groups representing unbranched skeletal parts produced 1,218 face groups. An analysis of these groups shows that many of them represent insignificantly small skeletal parts (cf. Fig. 10). Hence a second regularization step acting on these face groups and using the overall area of the group as significance measure has been done to clean up the skeleton. All groups with an overall area of less than 10 pixels have been removed if topological equivalence could be guaranteed. Thereafter 28,196 faces were left. Obviously this produced an additional number of edges joining only two elementary Voronoi faces. Hence the aggregation procedure has been repeated which led to 179 face groups. Figure 11 shows the resulting skeleton after the two regularization steps as a fusible stereo pair.

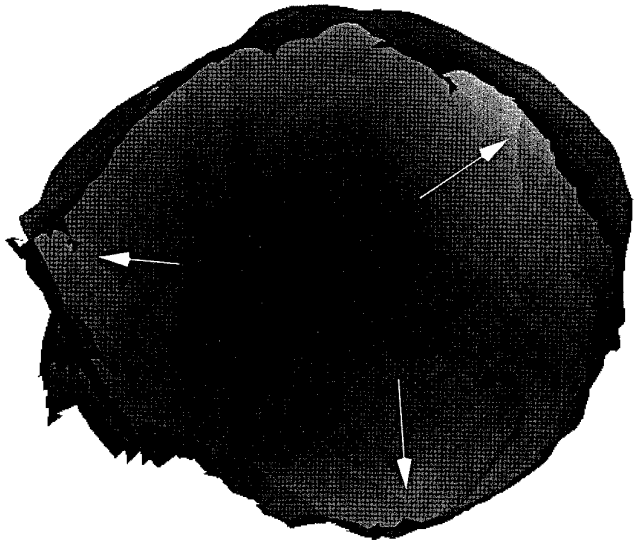

FIG. 12. The medial surface representing the acetabulum of the hip bone colored by the local bone thickness (growing from black to white). The arrows indicate thick bone areas which are optimal for prosthesis support.

For the visualization of the skeleton the use of elementary Voronoi faces is acceptable. However, for the representation and analysis of the 3D shape of the organ, the face groups which represent global medial surfaces are used.

Figure 12 shows the single medial surface that has been produced by the aggregation procedure and represents the acetabulum. The planning of surgical procedures require the identification of thick bone areas capable of supporting the hip joint replacement prosthesis. In order to visualize and identify such areas, the medial surface of the acetabulum has been colored by the local bone thickness. The well-visible light areas denote optimal regions for prosthesis support.

5.2. *Analysis of the Cortical Structure of the Brain*

Neuroanatomical and histological findings from postmortem brains, as well as *in vivo* findings from MRI studies, suggest the presence of morphological temporal lobe abnormalities in schizophrenia. To determine whether or not sulco-gyral pattern abnormalities in the temporal lobe could be detected *in vivo*, computerized surface rendering techniques for MR data have been developed in order to make qualitative and quantitative analysis of three-dimensional reconstruction of the temporal and frontal cortex. 3D renderings of the brain surface have been used to determine characteristics of the sulco-gyral patterns correlating with clinical findings [8].

One of the basic problems of this analysis was that the structural description of the brain surface has been derived from a single 2D view of the rendered data. This way the essentially 3D structure of the cortex has been coded and analyzed by view-dependent 2D descriptors setting serious limits for the subsequent analysis. The usage of real 3D shape features for the description of the cortical structures has been defined as the major preliminary for more precise and reliable statistical analysis of the data.

Skeletal representation offers a promising way to generate more precise descriptors of the sulco-gyral foldings. In

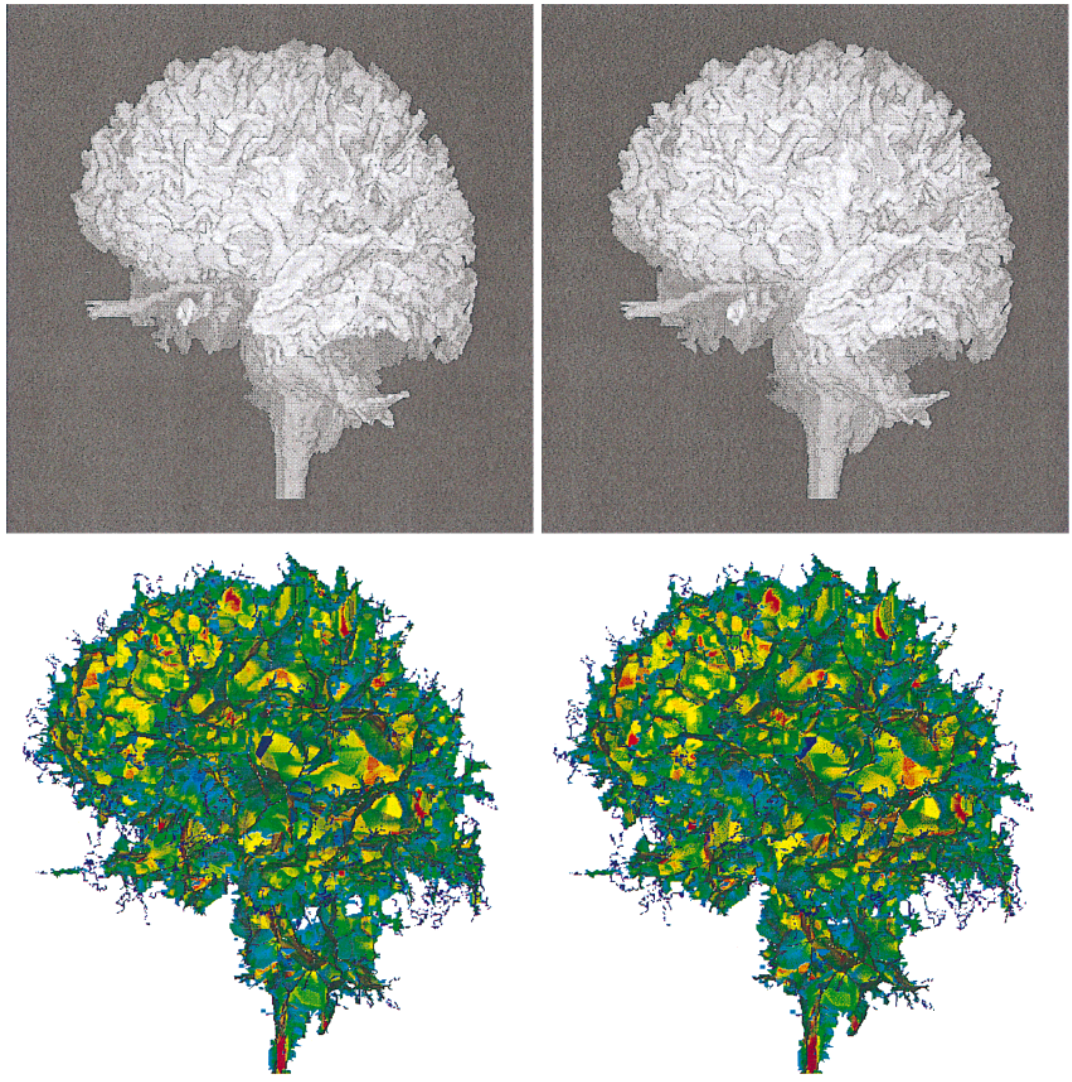

13

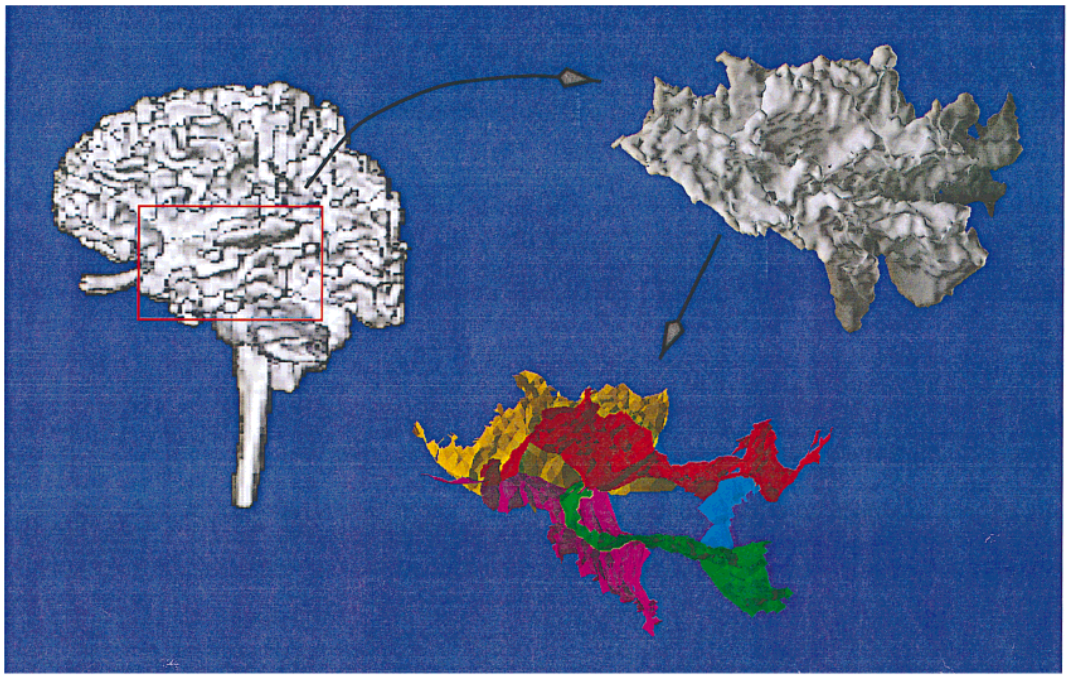

14

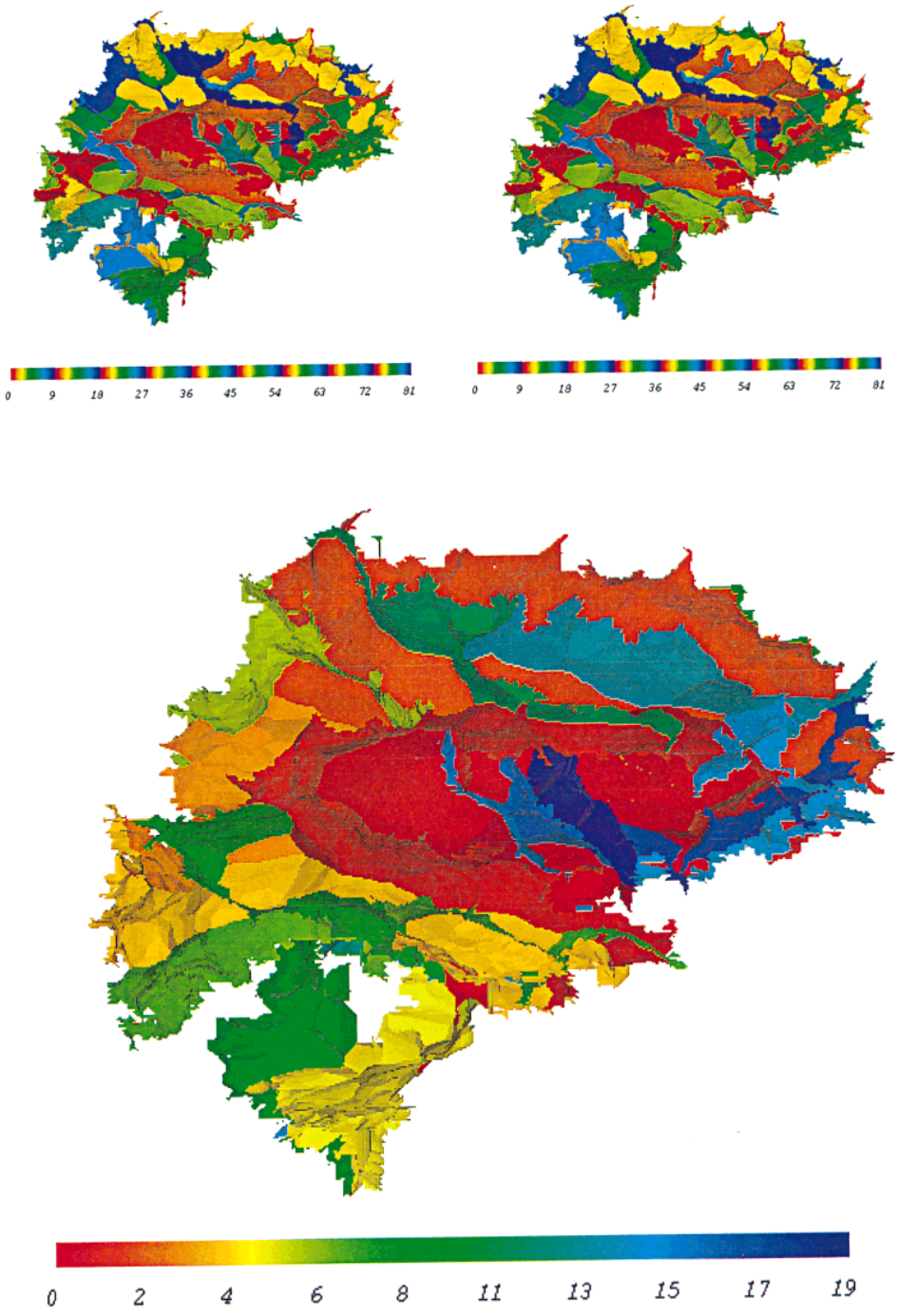

FIG. 15. Top row, the representation of the left inner cortical surface of a human brain shown as a fusible stereo pair. Different sheets have been assigned different colors according to the attached colormap. The bottom row shows the 20 most dominant skeletal sheets of the same object.

FIG. 13. Original object (top row) and 3D Voronoi skeleton (bottom row) of a human brain's white matter, shown as fusible stereo pairs. The skeletal faces are colored according to the importance measure (ridge strength of the DM growing from blue to red) used in the regularization process. The skeleton has been generated automatically using thresholding and Voronoi face grouping.

FIG. 14. Description of the gyral pattern of the left temporal lobe. On the left the rendering of the complete white matter surface is shown. The red box identifies the temporal lobe which has been cut out as shown by the top right figure. At the bottom, the extracted most prominent skeletal sheets corresponding to the major gyri of the temporal lobe are shown. The single colored sheets result from the manual postprocessing of the regularized skeleton.

our analysis the white brain matter extracted from an MR acquisition was processed by the skeletonization software. The data set contained 205,848 boundary points, which produced 300,563 Delaunay polyhedra and 488,504 elementary Voronoi faces. After regularization 87,205 elementary Voronoi faces were left. The original data and the resulting elementary Voronoi faces of the skeleton are shown as fusible stereo pair in Fig. 13. In this case the Voronoi faces are colored according to the importance measure (ridge strength of the DM) used in the regularization process.

The resulting skeletal structure is still very complex and cannot be directly used for the generation of 3D shape features without the extraction of a few dominant skeletal sheets. The result of such a postprocessing, similar to the one performed on the hip bone skeleton is demonstrated for the left temporal lobe by Fig. 14. In this example the temporal lobe of the brain under study has been manually extracted from the original white matter. The according 41,042 Voronoi faces have then been cut out from the complete VD of the whole white brain matter and processed by the double regularization as described in Section 5.1. After the first regularization step with the ridge-strength measure 16,319 faces were left. The aggregation led to 5,362 face groups and the deletion of the insignificantly small face groups reduced the number of faces to 10,684. These remaining Voronoi faces which now represent the skeleton of the temporal lobe are then aggregated a second time into face groups. Due to the heavily branched structure of the temporal cortex these face groups do not yet represent the final skeletal sheets. They must be further aggregated. This is done manually with the help of tools supporting the visualization of the face groups according to their size and neighborhood relations and the generation of a hierarchical ordering between them. This procedure results in a compact skeletal description from which the five most prominent skeletal branches have been selected to be displayed in Fig. 14.

While the manual postprocessing of the skeleton can be performed in about 10 min for this relatively simple example, similar analysis on a complete brain as illustrated in Fig. 15 may demand several hours of tedious manual work, which certainly limits the practical applicability of the package for such complex shapes and makes further development of the applied tools necessary. However, in case of atlas-based matching of brain structures in unsegmented images, such an analysis has to be performed only once, making the approach feasible even under the present conditions.

The shape of the cortical surface especially its gyration pattern is now coded in the branching of the individual skeletal sheets, clearly visible on the image. Current research is concentrating onto the extraction and quantitative description of the branching lines between neighboring skeletal sheets, leading to truly 3D descriptors of the sulcogyral structure of the temporal lobes.

6. CONCLUSIONS

We presented an overview about the conceptual, algorithmic, and practical aspects of the generation of 3D hierarchical skeletons and showed that while the basic ideas of Voronoi skeleton generation can be extended to 3D, several theoretical and algorithmic implementation problems arise. While the technical aspects of the 3D VD generation have been solved, regularization remains an open problem. This is basically due to the lack of a hierarchical organization of the Delaunay cells, providing no clue about a reasonable sequence for the deletion of the Delaunay polyhedra. Using some heuristics, however, the generation of 3D skeletons even for very large, complex objects proved to be possible. Very promising results have been presented for complex artificial data as well as anatomical objects as the hip bone or the human brain, extracted from high-resolution radiological acquisitions.

The 3D hierarchical skeleton promises to be an efficient tool for handling complex shapes of the human anatomy for object recognition as well as object shape characterization tasks. Combination of the Blum skeletal descriptors of binary objects with the recently proposed concept of the multi-scale medial axis concept applicable for gray-scale images opens a wide range of possible applications for skeletons in 2D and 3D scene analysis, capable to overcome fundamental difficulties caused by the selective use of symmetry axes during the medial axis transform.

The usability of skeletal sheets for solving shape-related tasks of morphological 3D organ analysis has been demonstrated by two prototypical applications in medical image analysis. The complex branching structure of skeletal sheets provides an appropriate representation of the underlying organ shape and can carry the information necessary for a subsequent quantitative analysis.

The presented work provides only a first step in the direction of skeleton based shape analysis. Further development is in progress allowing the generation of the complete skeletal hierarchy of the skeletons of anatomical objects. This hierarchy will allow us to concentrate selectively on the parts of the skeleton which are relevant to a specific application.

ACKNOWLEDGMENT

This work has been supported by Research Grant 2-77-938-94 of the Swiss National Science Foundation.

REFERENCES

1. D. Attali and A. Montanvert, Semicontinuous skeletons of 2D and 3D shapes, in *Proceedings, 2nd International Workshop on Visual Form*, World Scientific, Singapore, 1994, pp. 32–41.
2. H. Blum, A transformation for extracting new descriptors of shape, in *Models for the Perception of Speech and Visual Form* (W. Walthen-Dunn, Ed.), MIT Press, Cambridge, MA, 1967.
3. J. W. Brandt, Describing a solid with the three-dimensional skeleton, in *Proceedings SPIE Conference on Curves and Surfaces in Computer Vision and Graphics III, Boston 1992*, Vol. 1830, pp. 258–269.
4. J. W. Brandt and V. R. Algazi, Continuous skeleton computation by Voronoi Diagram, *CVGIP: Image Understanding* 1992, **55**(3), 329–338.
5. P. Cignoni, C. Montani, and R. Scopigno, *A Merge-First Divide & Conquer Algorithm for E^d Triangulations*, Technical Report 92-16, Istituto CNUCE-CNR, Pisa, Italy, 1992.
6. P. Danielsson, Euclidean distance mapping, *Comput. Vision Graphics Image Process.* **14,** 1980, 227–248.
7. M. Kass, A. Witkin, and D. Terzopoulos, Snakes: Active contour models, *Int. Conf. Comput. Vision*, June 1987, 259–268.
8. R. Kikinis, M. E. Shenton, G. Gerig, H. Hokama, J. Haimson, B. F. O'Donnel, C. G. Wible, R. W. McCarley, and F. A. Jolesz, Temporal lobe sulco-gyral pattern anomalies in schizophrenia: An MR three-dimensional surface rendering study, *Neurosci. Lett.* **182,** 1994, 7–12.
9. V. Kovalevsky, Finite topology as applied to image analysis, *Comput. Vision Graphics Image Process.* **46,** 1989, 141–161.
10. D. T. Lee, Medial axis transformation of a planar shape, *IEEE PAMI* **4**(4), 1982, 363–369.
11. F. Meyer, Skeletons and perceptual graphs, *Signal Process.* **16,** 1989, 335–363.
12. B. S. Morse, S. M. Pizer, and C. A. Burbeck, General shape and specific detail: Context-dependent use of scale in determining visual form, in *Proceeding 2nd International Workshop on Visual Form*, pp. 374–383, World Scientific, Singapore, 1994.
13. L. R. Nackman and S. M. Pizer, Three-dimensional shape description using the symmetric axis transformation. I. Theory, *IEEE PAMI* **7**(2), 1985, 187–202.
14. R. L. Ogniewicz and M. Ilg, Voronoi skeletons: Theory and applications, in *IEEE CVPR*, pp. 63–69, IEEE Comput. Soc. Press, Los Alamitos, CA, 1992.
15. F. P. Preparata and M. I. Shamos, *Computational Geometry*, Springer-Verlag, New York, 1985.
16. M. Schmitt, Some examples of algorithms analysis in computational geometry by means of mathematical morphological techniques, in *Lecture Notes in Computer Science: Geometry and Robotics*, Vol. 391, pp. 225–246, Springer-Verlag, Berlin, 1989.
17. G. L. Scott, S. C. Turner, and A. Zisserman, Using a mixed wave/diffusion process to elicit the symmetry set, *Image Vision Computing* **7**(1), 1989, 63–70.
18. G. Székely, Ch. Brechbühler, O. Kübler, R. L. Ogniewicz, and T. Budinger, Mapping the human cerebral cortex using 3D medial manifolds, in *Proceedings VBC, Chapel Hill, October 1994*, SPIE, Vol. 1808, pp. 130–144.
19. H. Talbot and L. Vincent, Euclidean skeletons and conditional bisectors, in *Proceedings, SPIE Conference on Medical Imaging. V. Image Processing*, *1992*, Vol. 1818, pp. 862–876.